MATERIALS SCIENCE

Nanoscale ferroelastic twins formed in strained $LaCoO_3$ films

Er-Jia Guo[1,2,3], Ryan Desautels[1], David Keavney[4], Manuel A. Roldan[5], Brian J. Kirby[6], Dongkyu Lee[1], Zhaoliang Liao[1], Timothy Charlton[1], Andreas Herklotz[1,7], T. Zac Ward[1], Michael R. Fitzsimmons[1,8]*, Ho Nyung Lee[1]*

Copyright © 2019 The Authors, some rights reserved; exclusive licensee American Association for the Advancement of Science. No claim to original U.S. Government Works. Distributed under a Creative Commons Attribution NonCommercial License 4.0 (CC BY-NC).

The coexistence and coupling of ferroelasticity and magnetic ordering in a single material offers a great opportunity to realize novel devices with multiple tuning knobs. Complex oxides are a particularly promising class of materials to find multiferroic interactions due to their rich phase diagrams, and are sensitive to external perturbations. Still, there are very few examples of these systems. Here, we report the observation of twin domains in ferroelastic $LaCoO_3$ epitaxial films and their geometric control of structural symmetry intimately linked to the material's electronic and magnetic states. A unidirectional structural modulation is achieved by selective choice of substrates having twofold rotational symmetry. This modulation perturbs the crystal field–splitting energy, leading to unexpected in-plane anisotropy of orbital configuration and magnetization. These findings demonstrate the use of structural modulation to control multiferroic interactions and may enable a great potential for stimulation of exotic phenomena through artificial domain engineering.

INTRODUCTION

Ferroelastics are the largest class of ferroic materials and are essential for many applications, such as vibration sensors, smart mechanical switches, and acoustic devices (*1*–*3*). Complex perovskite oxides with a rhombohedral lattice structure offer a particularly interesting subclass of ferroelastic materials. In this structure, the ferroelastic response is driven by a distortion of the cubic parent structure through stretching along one of the four body diagonals of the perovskite unit cell. To minimize the total elastic energy, ferroelastic oxides commonly form twin domains at the expense of interfacial energy associated with domain walls (*4*, *5*). Arrays of periodic domains have been reported in ferroelastic rare-earth phosphates (*1*, *3*, *6*–*8*) and aluminates (*3*, *5*, *9*, *10*). The ferroelastic domains walls passing through the single crystals are invariably arranged regularly because of the strain compatibility conditions between the adjacent domains, forming a quasi–one-dimensional (1D) domain configuration. The unique periodic ferroelastic domains have only been observed in the bulk previously. In addition, conventional ferroelastic materials also typically lack ferromagnetic ordering (*1*, *3*, *5*–*10*), which precludes direct coupling between the ferroelastic and ferromagnetic order parameters.

$LaCoO_3$ (LCO) is a ferroelastic perovskite oxide. Unlike bulk LCO, epitaxially strained LCO thin films (*11*, *12*) exhibit emergent ferromagnetism at low temperatures, recently attracting increasing attention (*13*–*19*). The delicate interplay between the crystal field splitting energy (Δ_{cf}) and interatomic exchange interaction energy (Δ_{ex}) determines the active spin crossover between low and high spin states of Co ions. Since Δ_{cf} is extremely sensitive to changes of Co—O bond length and Co—O—Co bonding angle (*18*, *19*), a small structural perturbation by strain can profoundly modify the Co spin state, thereby affecting the magnetism of LCO films. Misfit strain between an epitaxial ferroelastic thin film and a high–order symmetry substrate is accommodated in different ways. Typically, biaxial strain relaxation originating from the lattice mismatch proceeds through elastic deformation of the unit cell or the formation of misfit dislocations at the film and substrate interface. In contrast, misfit shear strain relaxes via spontaneous symmetry reduction of a film upon the ferroelastic transition, favoring the formation of ferroelastic domains (*11*). In the thin films, the orientation of ferroelastic domains is strongly influenced by the morphology of underlying substrates. For vicinal substrates, the miscut direction (α) and miscut angle (β) are two essential parameters that determine the in-plane domain configuration (Fig. 1A). For a large α, the fourfold symmetry of the (001) plane is broken into twofold by exposing both (010) and (100) facets at the terrace steps. Therefore, the ferroelastic thin films will have two possible in-plane epitaxial directions, resulting in multiple domain formation with random orientations. However, if α is close to zero, then ferroelastic thin films grow along a preferred direction [either (100) or (010)]; thus, the unidirectional structural twinning arrangement can be realized. Such an approach allows us to investigate the effect of a single structural modulation on the intriguing physical properties of ferroelastic thin films.

Here, using LCO as an example, we show the stabilization of 1D and checkerboard-like twinning domains in ferroelastic thin films by selecting the morphology and symmetry of underlying substrates. We demonstrate that a small change of the surface miscut direction or the choice of crystallographic symmetry play a crucial role in the formation of ferroelastic twin domains. The structural modulation induces a large anisotropy in the orbital occupancy, accompanied by an emergence of robust in-plane magnetic anisotropy. Our work strengthens the understanding of strong correlation between the ferroic order parameters of a multiferroic material.

RESULTS AND DISCUSSION

LCO thin films with a thickness of 35 unit cells (u.c.) were grown on (001)-oriented, TiO_2-terminated $SrTiO_3$ (STO), $(LaAlO_3)_{0.3}(SrAl_{0.5}Ta_{0.5}O_3)_{0.7}$

[1]Oak Ridge National Laboratory, Oak Ridge, TN 37831, USA. [2]Beijing National Laboratory for Condensed Matter Physics and Institute of Physics, Chinese Academy of Sciences, Beijing 100190, China. [3]Center of Materials Science and Optoelectronics Engineering, University of Chinese Academy of Sciences, Beijing 100049, China. [4]Advanced Photon Source, Argonne National Laboratory, Argonne, IL 60439, USA. [5]Eyring Materials Center, Arizona State University, Tempe, AZ 85287, USA. [6]NIST Center for Neutron Research, National Institute of Standards and Technology, Gaithersburg, MD 20899, USA. [7]Institute for Physics, Martin-Luther-University Halle-Wittenberg, Halle (Saale) 06120, Germany. [8]Department of Physics and Astronomy, University of Tennessee, Knoxville, TN 37996, USA.
*Corresponding author. Email: fitzsimmonsm@ornl.gov (M.R.F.); hnlee@ornl.gov (H.N.L.)

Downloaded from http://advances.sciencemag.org/ on August 23, 2019

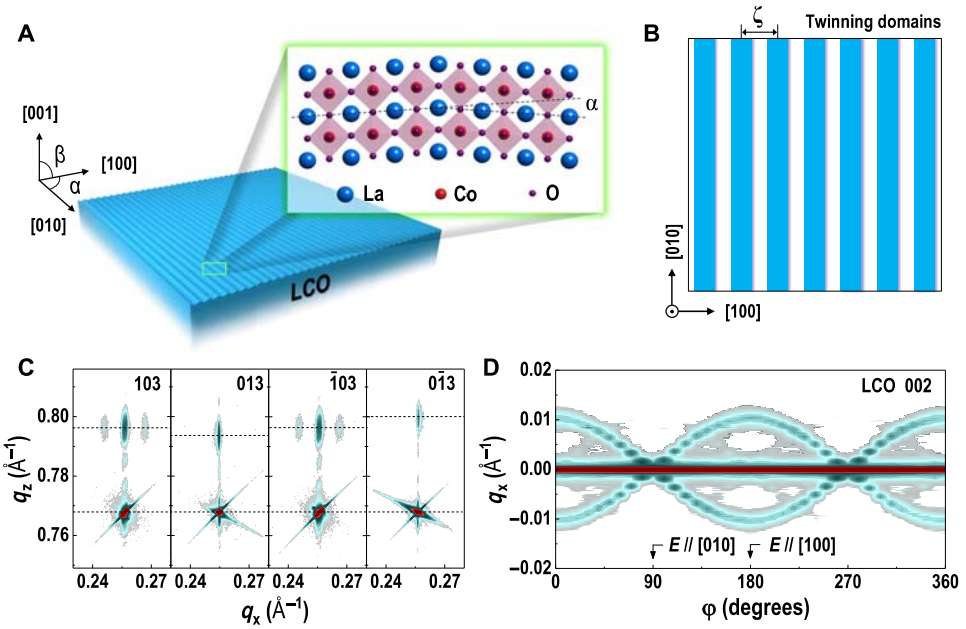

Fig. 1. 1D ferroelastic twinning domain is observed in an LCO thin film. (**A**) Schematic of 1D periodic twin domains. Twinning domains constitute a spatially unidirectional structural modulation along the [100] orientation. The domains are parallel to the step-edge direction of substrate. α and β are the miscut direction and miscut angle for a vicinal substrate, respectively. The inset shows a sketch of the monoclinically distorted LCO lattice at the ferroelastic domain wall. Notably, the tilt angle between two twin domains is γ = 2.2 ± 0.1°, derived from x-ray diffraction measurements (extended data fig. S1). (**B**) Top view of the stripe-like ferroelastic twin domains. Two different colors represent differently oriented ferroelastic domains with an average periodicity ζ. (**C**) Reciprocal space map (RSM) of an LCO film around the substrate's 103 reflection. RSMs are recorded by azimuthally rotating the sample with a step size of 90° with respect to the surface's normal. The LCO films have a monoclinically distorted lattice structure evidenced by the different q_z spacing between the film's peak and substrate's peak. Two splitting satellite reflections at the same q_z are shown for *h*03 reflections but are absent for 0*k*3 reflections. (**D**) Rocking curve scans around the LCO 002 reflections as a function of the in-plane rotation angle φ in a step of 10°. The real-space reflection angles are transformed into the reciprocal space wave vectors, from which we calculated $\zeta = 1/\Delta q_x \sim 10$ nm. A cosine modulation of the satellite peak position indicates that the domain structure is strictly aligned perpendicular to the [100] orientation.

(LSAT), and (110)-oriented $NdGaO_3$ (NGO) substrates by pulsed laser deposition (see Materials and Methods). The LCO films were subsequently capped with an ultrathin STO layer with a thickness of 5 u.c. to prevent the formation of nonstoichiometric surface due to oxygen vacancies (*17*, *20*). Results from x-ray diffraction (XRD) measurements confirm excellent epitaxial growth of all layers. Reciprocal space maps (RSMs) were measured around the film's 103 reflection (pseudocubic notation is used throughout the article) of an LCO film by azimuthally rotating the sample by 90° with respect to the surface's normal (Fig. 1C). RSM results confirm that the LCO film is coherently grown on the STO substrate. As the lattice parameter of STO is larger than that of bulk LCO, the LCO film is under biaxial tensile strain. The peak position of the 013 (or $0\bar{1}3$) reciprocal lattice reflection of the LCO film is shifted downward (or upward) along the *l*-direction with respect to the 103 and $\bar{1}03$ reflections. This result indicates that the symmetry of the LCO film grown on a cubic substrate changes from the bulk rhombohedral ($R\bar{3}c$) to a symmetric monoclinically distorted lattice structure ($I2/a$). The reflections of the LCO film show a central peak and two symmetric satellite peaks, which originate from ferroelastic twin domains. We find that the two satellite peaks only appear in the RSMs for the 103 and $\bar{1}03$ reflections, whereas the 013 and $0\bar{1}3$ reflections do not have these satellite peaks. Rocking curve scans around the LCO 002 reflection were recorded as a function of the in-plane rotation angle (φ) (Fig. 1D). A cosine-like modulation of the individual satellite peak position was observed. This observation confirms that the structural modulation is unidirectional. Furthermore, we only observe the first-order satellite peak of each 00*l* LCO reflection, indicating a rather short correlation length of twin domains. The angular difference (ω-ω_{00l}) between the central peaks and satellite peaks linearly reduces as the diffraction order (*l*) increases, revealing a constant in-plane structural modulation (*15*). We also measured RSMs around different *h*03 (*h* = 0, 1, 2, 3) reflections of the STO substrate (extended data fig. S1). The peak splitting of the LCO film along the *h*-direction is the same for all RSMs; however, no peak splitting occurs along the *l*-direction. This observation further reinforces the presence of a periodic structural modulation along the in-plane direction only (Fig. 1A). From the first-order rocking curve scan, we can obtain the tilt angle γ [=2.2(1)°] between two twin domains (extended data fig. S1). Moreover, by calculating the satellite spacing (Δq_x) between the central peaks and first-order satellite peaks, we can determine the periodicity ($\zeta = 1/\Delta q_x$) of twin domains to be ~10 nm (Fig. 1B). Note that the XRD results were obtained over a large portion of the sample (about tens of square millimeters), indicating that the 1D twin domains are prevalent throughout the LCO film.

To examine the correlation between the structural properties and surface morphology in our LCO films, the topography was measured over an area of 5 μm by 5 μm by atomic force microscopy (AFM) at several places across the sample (extended data fig. S2). All images show clear step-and-terrace patterns that are straight, continuous, and parallel to the [010] direction (*21*), i.e., $\alpha \approx 0$. We also find that ζ increases as β increases (extended data fig. S3). This is because the density of facet planes at steps increases with β; thus, the ferroelastic twin domains are more easily stabilized on the vicinal substrates with a larger β (*22*, *23*). In addition, ζ is approximately proportional to

Downloaded from http://advances.sciencemag.org/ on August 23, 2019

$t_{LCO}^{1/2}$ (extended data fig. S4C), where t_{LCO} is the film thickness, in accordance with thermodynamic consideration for domain formation in epitaxial ferroelastic films (*24*, *25*). The substrate morphology—as defined by α and β—controls the formation and arrangement of the unidirectional twin domains.

To explore the correlation between the electronic state and structural distortion in LCO films, we performed element-specific x-ray absorption spectroscopy (XAS) in total fluorescence yield (FY) mode. The features at the Co $L_{3,2}$-edge confirm that our films are oxygen stoichiometric with mixed spin-state Co^{3+} ions (*17*, *26*, *27*). The contribution from Co^{2+} ions induced by oxygen vacancies is negligible (<2%) in our films (*20*). X-ray linear dichroism (XLD) was measured to compare the difference in the electronic occupancy of Co d orbitals. To ensure that the observed linear dichroism is from the anisotropy in the e_g band, the measurements were taken under zero magnetic field (*28*). XLD measurements were performed with the x-ray scattering planes parallel to the (100) and (010) planes, respectively (Fig. 2A). The XAS intensities from the out-of-plane (E_{oop}//[001]) and in-plane (E_{ip}//[100] or [010]) linearly polarized x-ray beam are proportional to the density of unoccupied states, i.e., holes, in the Co $d_{3z^2-r^2}$ and $d_{x^2-y^2}$ orbitals, respectively (*26*–*28*). As shown in Fig. 2B, the peak energy of I_{ip} is lower than that of I_{oop}; thus, the occupation of d electrons in the $d_{x^2-y^2}$ orbital is larger compared to the $d_{3z^2-r^2}$ orbital. The difference in the peak positions between I_{ip} and I_{oop} implies a splitting of the e_g band arising from the $d_{x^2-y^2}$ and $d_{3z^2-r^2}$ orbitals (*28*). Direct inspection of the peak positions for XAS curves reveals that, for the (010) scattering geometry, I_{oop} is nearly the same as I_{ip}. For the (100) scattering geometry, the difference in the peak position between I_{oop}, and I_{ip} increases to ~0.15 eV, indicating a large e_g band splitting. These observations imply that the electronic configuration exhibits a notable anisotropy.

The difference between I_{oop} and I_{ip} is shown in Fig. 2C. The peak intensity of XLD spectra for the (010) scattering geometry is remarkably different from that of the (100) scattering geometry. To obtain a quantitative estimate of the imbalance in e_g band occupation, we applied the sum rule for linear dichroism to calculate the orbital polarization $P = (n_{x^2-y^2} - n_{3z^2-r^2}) / (n_{x^2-y^2} + n_{3z^2-r^2})$ (where $n_{x^2-y^2}$ and $n_{3z^2-r^2}$ represent the numbers of electrons) (*29*). P for the (010) scattering plane is ~27%, which is almost two times larger than that for the (100) scattering plane (~14%). The monoclinic distorted lattice will lead to a distortion of CoO_6 octahedral, e.g., changes of bonding angle and bond length, resulting in a strong anisotropy of electron occupancy along different planes. These observations are strong evidence that unidirectional structural modulation induces the large anisotropy in the electronic configuration, affecting both band splitting and orbital polarization in the Co d bands. In addition, we collected the total electron yield (TEY) spectra, which are known to be surface sensitive with a probing depth of ~3 to 5 nm. The results from the FY and TEY are identical, demonstrating that the strong anisotropy in the electronic states arises from the structural modulation of the entire LCO film and is not limited to the surface.

The unidirectional structural distortion has a strong influence on the magnetization (*M*) of LCO films. As shown in Fig. 3A, the *M* exhibits square-like hysteresis loops with magnetic field (*H*), corroborating the ferromagnetic order in tensile-strained LCO films (*13*–*17*). Hence, *M*(*H*) does not saturate even for fields of ± 7 T, suggesting an additional paramagnetic (PM) contribution. Previously, the PM component has been observed in LCO thin films and single crystals (*13*, *30*), where two magnetic sublattices contribute to the total magnetization. In-plane *M*(*H*) loops show clear anisotropy with a larger coercive field (H_C) and a higher *M* for *H* // [010] compared to those parameters for *H* // [100]. The inset of Fig. 3B shows the in-plane angular dependence of *M* at 10 and 70 K. A strong sine modulation of *M* is observed at 10 K with a maximum and minimum *M* along the [010] and [100] directions, respectively. The change of *M* is strongly correlated with the structural modulation. However, the variation in *M* is subtle at 70 K. *M* versus temperature (*T*) curves were measured while warming the sample with *H* // [010], [100], and [001], as shown in Fig. 3B. For *H* // [010], *M*(*T*) exhibits a sharp transition at the Curie temperature (T_C) of ~75 K (*13*–*17*). Unexpectedly, *M*(*T*) shows two distinct magnetic transitions when *H* // [100]: one at T_C and another at around 60 K. We note that the trends of *M*(*T*) curves are quite similar to each other for *H* // [100] and [001] when *T* < 60 K.

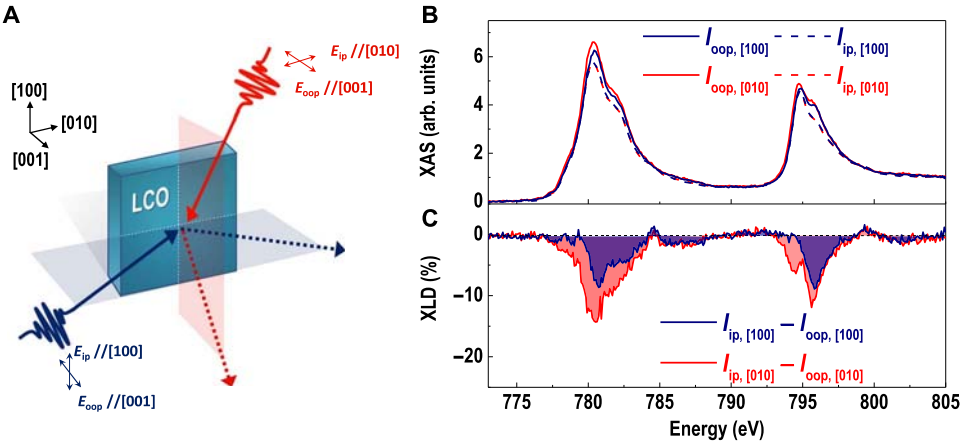

Fig. 2. Orbital polarization modulated by unidirectional structural distortions. (**A**). Schematic of the scattering geometry for XAS and XLD measurements with the x-ray beam aligned parallel to the (100) and (010) scattering planes. (**B**). XAS of an LCO film for the Co *L*-edge measured by the out-of-plane (I_{oop}, solid lines, E_{oop}//[001]) and in-plane (I_{ip}, dashed lines, E_{ip}//[100] or [010]) linearly polarized x-ray beams. (**C**) XLD of an LCO film for the Co *L*-edges. The XLD spectra indicate that the hole occupancy in the $d_{3z^2-r^2}$ orbital is larger than that of the $d_{x^2-y^2}$ orbital for both measuring configurations. The degree of orbital polarization in the (010) plane is about two times larger than that in the (100) plane, indicating a clear anisotropic orbital occupancy induced by 1D twin domains. All spectra are collected and repeated more than four times with bulk-sensitive FY detection mode at 10 K.

Downloaded from http://advances.sciencemag.org/ on August 23, 2019

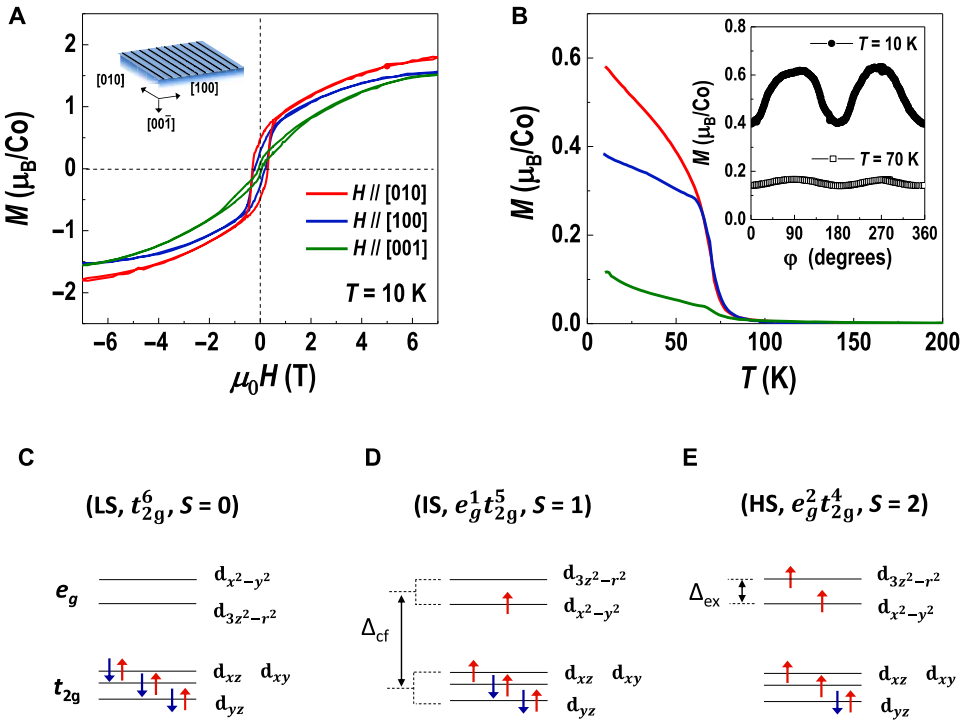

Fig. 3. In-plane magnetic anisotropy. (**A**) *M*(*H*) hysteresis loops and (**B**) *M*(*T*) curves measured from an LCO film with *H* applied along the [010], [100], and [001] directions. For the *M*(*T*) curves, the cooling field was set at 0.1 T, and the measurements were carried out during the sample warm up under a magnetic field of 0.1 T. The inset of (B) shows the angular dependence of the in-plane magnetization at 10 and 70 K under a magnetic field of 1 kOe. φ is the in-plane rotation angle with φ = 0° is *H* // [100] and φ = 90° is *H* // [010]. The in-plane magnetization is strongly modulated by the twin domain arrangement. (**C** to **E**) Schematic energy-level diagrams of Co^{3+} low-spin (LS), intermediate-spin (IS), and high-spin (HS) state configurations, respectively.

The unique magnetic behavior in our LCO films may be attributed to the unconventional electronic states triggered by the unidirectional structural modification. Since $\Delta_{cf} \neq 0$ for tensile-strained LCO films, the Co—O molecular orbitals are split into threefold degenerate t_{2g} and twofold degenerate e_g bands (Fig. 3, C to E). The electronic configuration, i.e., the spin state of Co ions, is controlled by the energy difference $\Delta E = \Delta_{cf} - \Delta_{ex} - W/2$, where W is the bandwidth (W) between the hybridized Co e_g orbital and the O 2p orbital. In unidirectionally distorted CoO_6 octahedra, the bond length (d) and bonding angle (δ) exhibit strong anisotropy; thus, both $W \propto \frac{\cos\delta}{d^{3.5}}$ and $\Delta_{cf} \propto \frac{1}{d^5}$ depend on crystallographic orientation (*31*–*33*). We thus expect the spin state of Co ions to depend on crystallographic orientation. The effective PM moments (μ_{eff}) ~ 4.67(3) and ~ 4.12(2) μ_B/Co (where μ_B is the Bohr magneton) were obtained from the susceptibilities above 100 K along the [010] and [100] orientations (Fig. 3B), respectively. Assuming a single-electron model, μ_{eff} is equal to $g_e\sqrt{S(S+1)}\,\mu_B$/Co, where the electron g factor $g_e = 2$. We calculate that the corresponding effective spin state of Co^{3+} ion is $S_{[010]} = 1.89(3)\ \mu_B$/Co and $S_{[100]} = 1.61(2)\ \mu_B$/Co. The large value of $S_{[010]}$ and $S_{[100]}$ can only be achieved with occupancies >89 and >61%, respectively, of high-spin (S = 2) Co ions. In addition, the XLD results demonstrate that the e_g band splitting along the [100] orientation is ~0.15 eV larger than that along the [010] orientation. Thus, electrons preferentially occupy the lower-energy orbitals, resulting in a higher spin state along the [010] orientation compared to that of the [100] orientation. These observations are consistent with the magnetization measurements.

To further illustrate the importance of the twofold rotational symmetry imposed by the substrates, we have grown LCO films on (110)-oriented orthorhombic $NdGaO_3$ (NGO) substrates (*19*, *34*). The in-plane lattice constants along the [$\bar{1}$10] and [001] orientations are different (Fig. 4A), providing anisotropic misfit strain intrinsic to the film. The structural anisotropy leads to an asymmetric LCO lattice structure, similar to LCO films grown on step-and-terrace STO substrates. XRD measurements confirm the formation of 1D twin domains in LCO films along the [$\bar{1}$10] orientation of NGO (extended data fig. S5). Therefore, the unidirectional structural distortion in LCO films can be achieved either by choice of a substrate morphology, i.e., α and β, or the choice of substrate crystallographic symmetry. Because of the strong PM background from NGO and the large coercive field of LCO films, the magnetic properties of LCO films cannot be easily quantified with magnetometry. The magnetization, however, can be elucidated by x-ray magnetic circular dichroism (XMCD) (*35*) and quantified with polarized neutron reflectometry (PNR) (*36*). Figure 4B shows XMCD spectra of the Co L-edges, with a magnetic field of 5 T applied along the [$\bar{1}$10] and [001] directions at 10 K. The difference in XMCD signals provides solid evidence for the in-plane anisotropy. A direct comparison of absolute magnetic moment along the two in-plane directions was obtained from PNR measurements at 10 K with a magnetic field of 3 T (extended data fig. S6). The nuclear (atomic density) and magnetization depth profiles of the LCO heterostructure are shown in Fig. 4 (C and D). The magnetic moment of the LCO film along the [001] orientation [0.70(5) μ_B/Co] is larger than that along the [$\bar{1}$10] orientation [0.54(2) μ_B/Co]. Both techniques reveal an appreciable difference in the magnetic responses along different in-plane directions, which offers further confirmation that the magnetic ground states are strongly modulated by

Downloaded from http://advances.sciencemag.org/ on August 23, 2019

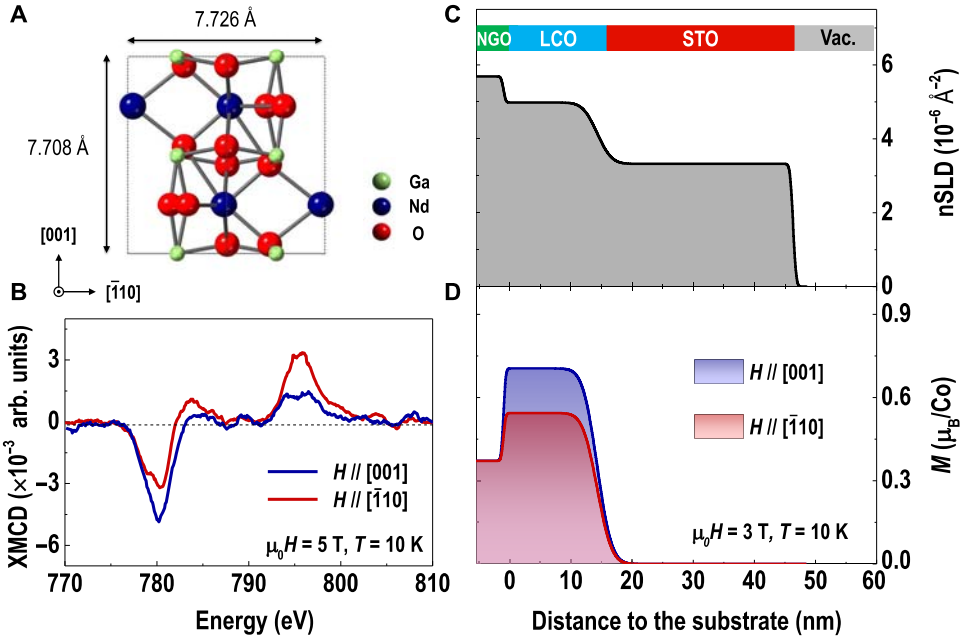

Fig. 4. In-plane magnetic anisotropy enforced by the orthorhombic substrate. (**A**) The top view lattice structure of orthorhombic (110)-oriented NGO. The in-plane lattice parameter along the [$\bar{1}$10] orientation is larger than that along the [001] orientation, leading to in-plane anisotropic shear strain in LCO films. (**B**) XMCD spectra for Co *L*-edge at 10 K with a magnetic field of 5 T applied along the [$\bar{1}$10] and [001] orientations. The XMCD signals were calculated from the difference between the μ^+ and μ^- divided by their sum, as described by $(\mu^+ - \mu^-)/(\mu^+ + \mu^-)$, where μ^+ and μ^- denote XAS obtained from the right- and left-hand circular polarized photons, respectively. (**C**) Nuclear scattering length density (nSLD) and (**D**) magnetic moment (derived from the magnetic scattering length density, mSLD) depth profiles of an LCO film. The inset of (**C**) shows the schematic of the sample geometry. The LCO film was grown on a NGO substrate and then capped with a STO thin layer to prevent loss of oxygen at the LCO surface. PNR measurements were performed at 10 K after field cooling in 3 T. The magnetic field was applied along the [$\bar{1}$10] and [001] orientations, respectively.

the orientation of unidirectional twin domains. Thus, choice of substrate symmetry and modification of surface morphology, which controls the periodicity and orientation of twin domains, are effective means to control the magnetic properties of LCO films.

Since we have found that the 1D twin domain formation originates from the terraced surfaces, one can hypothesize that diminishing step terrace features on a substrate may alter the formation of 1D twin domains. We were able to stabilize checkerboard-like twin domains in LCO films grown on a cubic LSAT substrate, which lacks a well-defined step-and-terrace surface because of cation segregation (extended data fig. S7). The formation of twin domains along both [010] and [100] directions were observed, confirming that the electronic states of LCO films exhibit a strong in-plane anisotropy with a reduced electron occupancy of the $d_{3z^2-r^2}$ orbital along the (110) plane (extended data fig. S8). The magnetic response for fields along the [100] and [010] orientations were identical, whereas the largest magnetization was observed with the field along the diagonal direction (extended data fig. S9). These observations further reinforce the strong correlation between structural distortion and electronic and magnetic ground states in strained LCO films.

Last, we demonstrate that artificially designed step-and-terrace morphology with perfectly aligned steps along either [010] or [100] orientation is essential for the formation of nanoscale 1D twin domains. A slight change in the miscut direction toward the diagonal direction modifies the area ratio between the (010) and (100) facet planes at the steps. If the substrate's surface is covered by two mixed facetted planes, then thin films will grow as orthogonally oriented checkerboard-like twin domains, yielding isotropic in-plane ferromagnetism (extended data fig. S10). The isotropic magnetization of these LCO films is determined by the average their volume from the maximum and minimum magnetizations of LCO films of individual domains.

CONCLUSIONS

In summary, we report the formation of ferroelastic twin domains in LCO epitaxial thin films by using substrate morphology and crystallographic symmetry. Surface-modified cubic substrates or orthorhombic substrates provide opportunities to achieve fine control of unidirectional structural modification, which provides fine control over the magnetic anisotropy. The competition between minimizing the elastic strain energy at the expense of the domain wall energy due to the induced twofold rotational symmetry leads to the formation of 1D twin domains. Our results demonstrate direct transfer of a unique symmetry-imposed domain pattern from the structure into the electronic state (orbital occupancy) and subsequent magnetic order. Using the control of domain architectures to investigate the strong correlation between different ferroic orders opens an avenue toward an improved fundamental understanding of the strongly correlated interactions for future functional device applications.

MATERIALS AND METHODS

Thin-film synthesis and physical property characterization

LCO thin films were grown by pulsed laser deposition. Before thin-film deposition, the STO (001) substrates and NGO (110) substrates

Downloaded from http://advances.sciencemag.org/ on August 23, 2019

were treated by buffered hydrofluoric acid and subsequent annealing at 1050°C for 2 hours to achieve atomically flat surfaces. The LSAT substrates were untreated because of cation segregation; thus, no specific termination and step-and-terrace are formed on LSAT substrates. During film growth, the substrate temperature was kept at 700°C, the oxygen partial pressure was maintained at 100 mTorr, and the laser fluence was fixed at ~1.2 J cm^{-2}. LCO films (~35 u.c.) grown on STO and LSAT were capped with an ultrathin STO layer (~5 u.c.) to prevent the formation of oxygen vacancies at the surface. LCO films (~80 u.c.) were grown on NGO and further capped with an STO layer (~80 u.c.) for the neutron reflectivity measurements. After growth, the samples were cooled to room temperature in 100 Torr of oxygen to ensure the right oxygen stoichiometry. X-ray reflectivity (XRR) measurements were performed to check the layer thickness and interface abruptness. The crystalline quality of all layers was checked by XRD θ-2θ and rocking curve scans. The in-plane strain states of the films were characterized by XRD RSM. The morphologies of substrates and samples were characterized with a Nanoscope III AFM in the tapping mode. The magnetic properties of LCO films were measured using a SQUID magnetometer (Quantum Design). The magnetization of LCO films was acquired by subtracting the diamagnetic signals from the substrates (STO and LSAT).

Soft XAS

XAS experiments were performed at beamline 4-ID-C of the Advanced Photon Source at Argonne National Laboratory. The valence state of Co ions in the as-grown LCO films was directly probed by XAS. XAS spectra near the Co *L*-edges were measured with bulk-sensitive FY and surface-sensitive TEY modes at 10 K. The incident angle between the x-ray beam and sample's surface plane is around 30°. XLD was measured by linearly polarized x-rays with polarization vector (E) parallel to the in-plane or out-of-plane direction of the sample, respectively. XMCD measurements were performed under an in-plane magnetic field of ± 5 T. The XMCD signals were calculated from the difference in the absorption of the right- and left-hand circularly polarized x-rays. The XMCD signal flips its polarity with reversal of applied magnetic field, indicating that the tensile-strained LCO films are magnetic in origin. The XMCD signals were corrected by multiplying 96%/cos(30°) ~ 1.1, with consideration given to the incident angle (30°) and circular polarization (96%) of the x-ray beam. XLD and XMCD measurements were repeated by successively rotating the sample by 90°, e.g., along two perpendicular in-plane orientations of the films.

Polarized neutron reflectometry

PNR experiments on LCO films grown on NGO substrates were performed at the polarized beam reflectometer (PBR) beamline of the National Institute of Standards and Technology (NIST) Center for Neutron Research (NCNR). The samples were field-cooled and measured with magnetic fields of 0.7 T (results were not shown) and 3 T, respectively. The magnetic fields were applied along the in-plane directions, e.g., [001] and [$\bar{1}$10], of the NGO substrate. PNR measurements were conducted at 10 K in the specular reflection geometry with the wave vector transfer (q) perpendicular to the sample's surface plane. We measured the spin-up (R^+) and spin-down (R^-) neutron reflectivity as a function of q ($=4\pi \sin\theta_i/\lambda$), where θ_i is the incident angle of neutrons and λ is the neutron wavelength. The neutron reflectivity was normalized to the asymptotic value of the Fresnel reflectivity R_F ($=16\pi^2/q^4$) to better illustrate the difference between R^+ and R^-, using presented spin-asymmetry SA ($= [(R^+ - R^-)/(R^+ + R^-)]$). The neutron data are shown in the Supplementary Materials. Data fitting was performed using both GenX and NIST Refl1D program (*37*). The results from two fitting programs are in good agreement. We constrained our chemical depth profile from fitting a model to XRR data to deduce the magnetization depth profile of the samples. The in-plane magnetization of LCO films along the [001] and [$\bar{1}$10] orientations can be quantitatively determined.

SUPPLEMENTARY MATERIALS

Supplementary material for this article is available at http://advances.sciencemag.org/cgi/content/full/5/3/eaav5050/DC1

Fig. S1. Structural properties of an LCO film.
Fig. S2. Topography of an LCO film capped with an STO ultrathin layer.
Fig. S3. Evolution of the 1D twin domain in LCO films grown on STO substrates with different miscut angles.
Fig. S4. Thickness-dependent twin domain periodicity in LCO films.
Fig. S5. 1D twin domain in LCO films grown on NGO substrates.
Fig. S6. In-plane magnetic anisotropy in LCO films grown on NGO substrate.
Fig. S7. Checkerboard-like twin domains observed in LCO films on LSAT substrates.
Fig. S8. Magnetic properties of LCO film on LSAT substrate with checkerboard-like twin domains.
Fig. S9. Anisotropic electronic states in LCO films on LSAT substrates.
Fig. S10. Comparison of the in-plane magnetic anisotropy in LCO films with and without (w.o.) 1D twin domains.

REFERENCES AND NOTES

1. V. K. Wadhawan, Ferroelasticity and related properties of crystals. *Phase Transit.* **3**, 3–103 (1982).
2. V. Nagarajan, A. Roytburd, A. Stanishevsky, S. Prasertchoung, T. Zhao, L. Chen, J. Melngailis, O. Auciello, R. Ramesh, Dynamics of ferroelastic domains in ferroelectric thin films. *Nat. Mater.* **2**, 43–47 (2003).
3. E. K. H. Salje, Ferroelastic materials. *Annu. Rev. Mater. Res.* **42**, 265–283 (2012).
4. A. L. Roitburd, Equilibrium structure of epitaxial layers. *Phys. Status Solidi A* **37**, 329–339 (1976).
5. S. Bueble, K. Knorr, E. Brecht, W. W. Schmahl, Influence of the ferroelastic twin domain structure on the {100} surface morphology of $LaAlO_3$ HTSC substrates. *Surf. Sci.* **400**, 345–355 (1998).
6. S. W. Meeks, B. A. Auld, Periodic domain walls and ferroelastic bubbles in neodymium pentaphosphate. *Appl. Phys. Lett.* **47**, 102–104 (1985).
7. B. Wruck, E. K. H. Salje, M. Zhang, T. Abraham, U. Bismayer, On the thickness of ferroelastic twin walls in lead phosphate $Pb_3(PO_4)_2$ an x-ray diffraction study. *Phase Transit.* **48**, 135–148 (1994).
8. X. R. Huang, S. S. Jiang, X. B. Hu, X. Y. Xu, W. Zeng, D. Feng, J. Y. Wang, One-dimensional behavior of ferroelastic domain arrays in neodymium pentaphosphate. *Phys. Rev. B* **52**, 9932–9937 (1995).
9. C.-H. Kim, S.-Y. Cho, I.-T. Kim, W.-J. Cho, K.-S. Hong, Twin structures in lanthanum, praseodymium, and neodymium aluminate ceramics. *Mater. Res. Bull.* **36**, 1561–1571 (2001).
10. R. J. Harrison, S. A. T. Redfern, E. K. H. Salje, Dynamical excitation and anelastic relaxation of ferroelastic domain walls in $LaAlO_3$. *Phys. Rev. B* **69**, 144101 (2004).
11. P. E. Vullum, R. Holmestad, H. L. Lein, J. Mastin, M. A. Einarsrud, T. Grande, Monoclinic ferroelastic domains in $LaCoO_3$-based perovskites. *Adv. Mater.* **19**, 4399–4403 (2007).
12. P. E. Vullum, H. L. Lein, M.-A. Einarsrud, T. Grande, R. Holmestad, TEM observations of rhombohedral and monoclinic domains in $LaCoO_3$-based ceramics. *Philos. Mag.* **88**, 1187–1208 (2008).
13. D. Fuchs, C. Pinta, T. Schwarz, P. Schweiss, P. Nagel, S. Schuppler, R. Scheider, M. Merz, G. Roth, H. v. Löhneysen, Ferromagnetic order in epitaxially strained $LaCoO_3$ thin films. *Phys. Rev. B* **75**, 144402 (2007).
14. D. Fuchs, E. Arac, C. Pinta, S. Schuppler, R. Schneider, H. v. Löhneysen, Tuning the magnetic properties of $LaCoO_3$ thin films by epitaxial strain. *Phys. Rev. B* **77**, 014434 (2008).
15. D. Fuchs, L. Dieterle, E. Arac, R. Eder, P. Adelmann, V. Eyert, T. Kopp, R. Schneider, D. Gerthsen, H. v. Löhneysen, Suppression of the ferromagnetic state in $LaCoO_3$ films by rhombohedral distortion. *Phys. Rev. B* **79**, 024424 (2009).
16. A. Herklotz, A. D. Rata, L. Schultz, K. Dörr, Reversible strain effect on the magnetization of $LaCoO_3$ films. *Phys. Rev. B* **79**, 092409 (2009).

Downloaded from http://advances.sciencemag.org/ on August 23, 2019

17. W. S. Choi, J.-H. Kwon, H. Jeen, J. E. Hamann-Borrero, A. Radi, S. Macke, R. Sutarto, F. He, G. A. Sawatzky, V. Hinkov, M. Kim, H. N. Lee, Strain-induced spin states in atomically ordered cobaltites. *Nano Lett.* **12**, 4966–4970 (2012).
18. J.-S. Zhou, J.-Q. Yan, J. B. Goodenough, Bulk modulus anomaly in $RCoO_3$ (R=La, Pr, and Nd). *Phys. Rev. B* **71**, 220103 (2005).
19. T. Vogt, J. A. Hriljac, N. C. Hyatt, P. Woodward, Pressure-induced intermediate-to-low spin state transition in $LaCoO_3$. *Phys. Rev. B* **67**, 140401 (2003).
20. J. E. Hamann-Borrero, S. Macke, W. S. Choi, R. Sutarto, F. He, A. Radi, I. Elfimov, R. J. Green, M. W. Haverkort, V. B. Zabolotnyy, H. N. Lee, G. A. Sawatzky, V. Hinkov, Valence-state reflectometry of complex oxide heterointerfaces. *npj Quantum Mater.* **1**, 16013 (2016).
21. M. Lippmaa, N. Nakagawa, M. Kawasaki, S. Ohashi, H. Koinuma, Growth mode mapping of $SrTiO_3$ epitaxy. *Appl. Phys. Lett.* **76**, 2439 (2000).
22. Q. Gan, R. A. Rao, C. B. Eom, Control of the growth and domain structure of epitaxial $SrRuO_3$ thin films by vicinal (001) $SrTiO_3$ substrates. *Appl. Phys. Lett.* **70**, 1962 (1997).
23. Y.-H. Chu, M. P. Cruz, C.-H. Yang, L. W. Martin, P.-L. Yang, J.-X. Zhang, K. Lee, P. Yu, L.-Q. Chen, R. Ramesh, Domain control in multiferroic $BiFeO_3$ through substrate vicinality. *Adv. Mater.* **19**, 2662–2666 (2007).
24. F. Sandiumenge, J. Santiso, L. Balcells, Z. Konstantinovic, J. Roqueta, A. Pomar, J. P. Espinós, B. Martínez, Competing misfit relaxation mechanisms in epitaxial correlated oxides. *Phys. Rev. Lett.* **110**, 107206 (2013).
25. C. Kittel, Theory of the structure of ferromagnetic domains in films and small particles. *Phys. Rev.* **70**, 965–971 (1946).
26. N. P. Lu, P. Zhang, Q. Zhang, R. Qiao, Q. He, H.-B. Li, Y. J. Wang, J. W. Guo, D. Zhang, Z. Duan, Z. L. Li, M. Wang, S. Z. Yang, M. Z. Yan, E. Arenholz, S. Y. Zhou, W. L. Yang, L. Gu, C. W. Nan, J. Wu, Y. Tokura, P. Yu, Electric-field control of tri-state phase transformation with a selective dual-ion switch. *Nature* **546**, 124–128 (2017).
27. M. W. Haverkort, Z. Hu, J. C. Cezar, T. Burnus, H. Hartmann, M. Reuther, C. Zobel, T. Lorenz, A. Tanaka, N. B. Brookes, H. H. Hsieh, H.-J. Lin, C. T. Chen, L. H. Tjeng, Spin state transition in $LaCoO_3$ studied using soft x-ray absorption spectroscopy and magnetic circular dichroism. *Phys. Rev. Lett.* **97**, 176405 (2006).
28. E. Benckiser, M. W. Haverkort, S. Brück, E. Goering, S. Macke, A. Frañó, X. P. Yang, O. K. Anderson, G. Cristiani, H.-U. Habermeier, A. V. Boris, I. Zegkinoglou, P. Wochner, H.-J. Kim, V. Hinkov, B. Keimer, Orbital reflectometry of oxide heterostructures. *Nat. Mater.* **10**, 189–193 (2011).
29. G. van der Laan, Sum rules and fundamental spectra of magnetic x-ray dichroism in crystal field symmetry. *J. Phys. Soc. Jpn.* **63**, 2393–2400 (1994).
30. J.-Q. Yan, J.-S. Zhou, J. B. Goodenough, Ferromagnetism in $LaCoO_3$. *Phys. Rev. B* **70**, 014402 (2004).
31. C. Pinta, D. Fuchs, M. Merz, M. Wissinger, E. Arac, H. v. Löhneysen, A. Samartsev, P. Nagel, S. Schuppler, Suppression of spin-state transition in epitaxially strained $LaCoO_3$. *Phys. Rev. B* **78**, 174402 (2008).
32. G. E. Sterbinsky, R. Nanguneri, J. X. Ma, J. Shi, E. Karapetrova, J. C. Woicik, H. Park, J.-W. Kim, P. J. Ryan, Ferromagnetism and charge order from a frozen electron configuration in strained epitaxial $LaCoO_3$. *Phys. Rev. Lett.* **120**, 197201 (2018).
33. Y. Yokoyama, Y. Yamasaki, M. Taguchi, Y. Hirata, K. Takubo, J. Miyawaki, Y. Harada, D. Asakura, J. Fujioka, M. Nakamura, H. Daimon, M. Kawasaki, Y. Tokura, H. Wadati, Tensile-strain-dependent spin states in epitaxial $LaCoO_3$ thin films. *Phys. Rev. Lett.* **120**, 206402 (2018).
34. Z. Liao, M. Huijben, Z. Zhong, N. Gauquelin, S. Macke, R. J. Green, S. Van Aert, J. Verbeeck, G. Van Tendeloo, K. Held, G. A. Sawatzky, G. Koster, G. Rijnders, Controlled lateral anisotropy in correlated manganite heterostructures by interface-engineered oxygen octahedral coupling. *Nat. Mater.* **15**, 425–431 (2016).
35. G. Schütz, W. Wagner, W. Wilhelm, P. Kienle, R. Zeller, R. Frahm, G. Materlik, Absorption of circularly polarized x rays in iron. *Phys. Rev. Lett.* **58**, 737–740 (1987).
36. M. R. Fitzsimmons, S. D. Bader, J. A. Borchers, G. P. Felcher, J. K. Furdyna, A. Hoffmann, J. B. Kortright, I. K. Schuller, T. C. Schulthess, S. K. Sinha, M. F. Toney, D. Weller, S. Wolf, Neutron scattering studies of nanomagnetism and artificially structured materials. *J. Magn. Magn. Mater.* **271**, 103–146 (2004).
37. B. J. Kirby, P. A. Kienzle, B. B. Maranville, N. F. Berk, J. Krycka, F. Heinrich, C. F. Majkrzak, Phase-sensitive specular neutron reflectometry for imaging the nanometer scale composition depth profile of thin-film materials. *Curr. Opin. Colloid Interface Sci.* **17**, 44–53 (2012).

Acknowledgments: We thank Y. Liu, F. Ye, C. Sohn, H. Jeen, J. K. Keum, and F. A. Reboredo for valuable discussions. **Funding:** This work was supported by the U.S. Department of Energy (DOE), Office of Science, Basic Energy Sciences, Materials Sciences and Engineering Division. T.Z.W. acknowledges the support by the U.S. DOE Office of Science, Early Career Research Program. The PNR measurements at the NCNR, U.S. Department of Commerce were performed via a user proposal. This research used resources of the Advanced Photon Source, a U.S. DOE Office of Science User Facility, operated for the DOE Office of Science by Argonne National Laboratory under contract no. DE-AC02-06CH1135 (XAS). During the manuscript revision, E.-J.G. was funded through the Hundred Talent Program of Chinese Academy of Sciences. **Author contributions:** H.N.L. directed the project. E.-J.G. and D.L. grew thin-film samples, and E.-J.G. carried out the structural and magnetic property measurements. E.-J.G., R.D., and D.K. performed the XAS experiments. E.-J.G. and B.J.K conducted the PNR measurements. D.L., M.A.R., Z.L., A.H., T.C., T.Z.W., M.R.F., and H.N.L. contributed to the data analysis and interpretation. E.-J.G., M.R.F., and H.N.L. wrote the manuscript with contributions from all the coauthors. **Competing interests:** The authors declare that they have no competing interests. **Data and materials availability:** All data needed to evaluate the conclusions in the paper are present in the paper and/or the Supplementary Materials. Additional data related to this paper may be requested from the authors. Supplementary information is available in the online version of the paper. Reprints and permissions information is available online. Certain commercial equipment is identified in this paper to foster understanding. Such identification does not imply recommendation or endorsement by NIST nor does it imply that the materials or equipment identified are necessarily the best available for the purpose.

Submitted 22 September 2018
Accepted 6 February 2019
Published 29 March 2019
10.1126/sciadv.aav5050

Citation: E.-J. Guo, R. Desautels, D. Keavney, M. A. Roldan, B. J. Kirby, D. Lee, Z. Liao, T. Charlton, A. Herklotz, T. Zac Ward, M. R. Fitzsimmons, H. N. Lee, Nanoscale ferroelastic twins formed in strained $LaCoO_3$ films. *Sci. Adv.* **5**, eaav5050 (2019).

Downloaded from http://advances.sciencemag.org/ on August 23, 2019

Science Advances

Nanoscale ferroelastic twins formed in strained $LaCoO_3$ films

Er-Jia Guo, Ryan Desautels, David Keavney, Manuel A. Roldan, Brian J. Kirby, Dongkyu Lee, Zhaoliang Liao, Timothy Charlton, Andreas Herklotz, T. Zac Ward, Michael R. Fitzsimmons and Ho Nyung Lee

Sci Adv **5** (3), eaav5050.
DOI: 10.1126/sciadv.aav5050

ARTICLE TOOLS http://advances.sciencemag.org/content/5/3/eaav5050

SUPPLEMENTARY MATERIALS http://advances.sciencemag.org/content/suppl/2019/03/25/5.3.eaav5050.DC1

REFERENCES This article cites 37 articles, 0 of which you can access for free
http://advances.sciencemag.org/content/5/3/eaav5050#BIBL

PERMISSIONS http://www.sciencemag.org/help/reprints-and-permissions

Use of this article is subject to the Terms of Service

Science Advances (ISSN 2375-2548) is published by the American Association for the Advancement of Science, 1200 New York Avenue NW, Washington, DC 20005. 2017 © The Authors, some rights reserved; exclusive licensee American Association for the Advancement of Science. No claim to original U.S. Government Works. The title *Science Advances* is a registered trademark of AAAS.

Downloaded from http://advances.sciencemag.org/ on August 23, 2019